Preprints, *24th Conf. on Severe Local Storms*, Amer. Meteor. Soc., Savannah, GA, October 2008.

P3.5 IMPACT OF A TORNADO'S LOW–REFLECTIVITY EYE ON DISTORTING THE ASSOCIATED PEAK DOPPLER VELOCITY MEASUREMENTS: A SIMULATION STUDY

Rodger A. Brown and Vincent T. Wood
NOAA/National Severe Storms Laboratory, Norman, OK

David C. Dowell
National Center for Atmospheric Research, Boulder, CO

1. INTRODUCTION

Weather radars located within a few tens of kilometers of a significant tornado reveal the presence of a weak reflectivity "eye" centered on the tornado (e.g., Fujita and Wakimoto 1982; Wakimoto and Martner 1992; Wurman et al. 1996: Wakimoto et al. 1996; Wurman and Gill 2000; Bluestein and Pazmany 2000; Wakimoto et al. 2003; Bluestein et al. 2003; Bluestein et al. 2004; Alexander and Wurman, 2005). The eye arises from the centrifuging of debris and hydrometeors within the tornadic circulation.

Using the axisymmetric numerical model of Dowell et al. (2005), Brown et al. (2006) produced flow and reflectivity patterns for three different–sized simulated tornadoes. The model output then was scanned with a WSR–88D emulator to produce simulated reflectivity and mean Doppler velocity measurements within the tornadoes. The results show that the extreme mean Doppler velocity values associated with a low-reflectivity eye at relatively close ranges occur at a smaller radius than that of the peak tangential velocities in the model tornado. The simulations indicate that this anomalous situation is not very evident in small tornadoes, but occurs out to ranges of 15–20 km for large tornadoes and out to 30–40 km for very large tornadoes using legacy WSR–88D sampling. With the new higher–density super–resolution WSR–88D sampling, the range to which the anomalies are evident increases by nearly 50%.

In this paper, we demonstrate why peak Doppler velocity measurements made in a tornado with a low–reflectivity eye occur closer to the tornado center than do the tornado's actual peak tangential velocities.

2. METHOD

a. Numerical tornado model

The Dowell et al. (2005) model used in this study consists of axisymmetric forced convection (buoyant bubble along the central axis) inside a closed impermeable cylinder that rotates with a constant angular velocity (Fiedler 1993). As the central updraft develops, air converging into the lower portion of the domain experiences an increase in tangential velocity, leading to the development of a tornado. In this way, an axisymmetric (two-dimensional) representation of a fully three–dimensional flow field develops consisting of evolving radial, vertical, and tangential velocity components.

The model permits objects (debris and hydrometeors) to be moved and centrifuged by the flow field. Each sized object has its own specified terminal fall velocity. We chose to include only a single size of hydrometeor in our experiments. Since the sizes of hydrometeors within tornadoes are not known, we found, after experimenting with various–sized raindrops, that the centrifuging of 1.5 mm diameter drops (terminal fall velocity of 5.4 m s^{-1}) produced realistic weak-reflectivity eyes. From their experiments, Dowell et al. (2005) deduced that raindrops with fall velocities less than 10 m s^{-1} likely are the dominant radar scatterers within tornadoes.

b. Doppler radar emulator

WSR–88D reflectivity and Doppler velocity measurements in the model tornadoes were simulated using a Doppler radar emulator that reproduced the basic characteristics of a WSR–88D, but several simplifications were employed. Instead of the radar beam consisting of a main lobe and side lobes, it consisted only of a main lobe that was represented by a Gaussian distribution having a width of three half-power beamwidths (Fig. 1). Doppler velocity values were computed from the Doppler component of the three–dimensional model raindrop motion. Rather than computing mean Doppler velocity and reflectivity values from a given number of pulses, the values were computed from Gaussian–weighted model Doppler velocity and reflectivity values within the radar beam. To compensate for antenna rotation in the azimuthal direction during the time it takes to collect the required number of samples, the horizontal dimension of the beam was represented by a broadened *effective* half–power beamwidth (EBW). The effective half–power beamwidth is specified by the azimuthal sampling interval, which in turn is specified by the number of pulses, pulse repetition frequency, and antenna rotation rate (e.g., Doviak and Zrnić 1993, pp. 193–197).

Doppler radar data were simulated using two different WSR–88D spatial resolutions: (1) the original legacy resolution and (2) the new super resolution (Fig. 2). Using legacy resolution, WSR–88Ds process and display data at 1.0^{o} azimuthal intervals; the range interval for reflectivity is 1.0 km and for Doppler velocity is 0.25 km. For super–resolution data collection, both Doppler velocity and reflectivity data are processed at 0.5^{o} azimuthal and 0.25 km range intervals. Using the National Severe Storms Laboratory's test bed WSR-88D (KOUN), Brown et al. (2005) showed that actual

reflectivity and Doppler velocity signatures in severe storms are more clearly depicted with super–resolution data.

3. RESULTS

Three different tornadoes were created using the numerical tornado model. In Experiment I (EXP I), a medium–sized tornado was produced (peak tangential velocity of 32 m s^{-1} at a core radius of 75 m at 1.0 km height). In Experiment II (EXP II), a large tornado was produced (peak velocity of 62 m s^{-1} at core radius of 165 m at 1.0 km), while Experiment III (EXP III) generated a very large tornado (peak velocity of 64 m s^{-1} at core radius of 340 m at 1.0 km). In this paper, we discuss only the large tornado from EXP II. All three experiments are discussed by Wood et al. (2009).

As an introduction to the influence of the distribution of radar scatterers on Doppler velocity measurements across a tornado, Fig. 3 was prepared. Examples of simulated Doppler velocity and reflectivity profiles in the radial direction from the center of the EXP II tornado for the two Doppler radar data resolutions are presented at a height of 2.0 km and at various ranges from the simulated radar. In order to present continuous Doppler velocity and reflectivity profiles, values were calculated as if the radar were able to make measurements at infinitesimally small azimuth intervals.

If the radar beamwidth was zero (i.e., perfect resolution), Doppler velocity and reflectivity measurements would have perfectly reproduced the model tangential velocity and reflectivity values in the tornado, as indicated by the thick gray curves in Fig. 3. However, with effective beamwidths of 1.02º for super–resolution azimuthal sampling (left side of Fig. 3) and 1.39º for legacy sampling (right side), reflectivity and Doppler velocity profiles become degraded, and increasingly so, as the beam broadens with increasing range from the radar.

With super-resolution sampling of the EXP II vortex, the weak-reflectivity eye and surrounding higher–reflectivity annulus (Fig. 3a) gradually disappear with increasing range, transforming essentially into a uniform reflectivity field beyond a range of about 50 km. In contrast, the reflectivity field produced by legacy–resolution sampling is nearly uniform at all ranges (Fig. 3b). The reason for the marked differences resulting from the two sampling resolutions is evident in Fig. 2. The reflectivity sampling volume for legacy resolution is 1.0º by 1.0 km, whereas, the sampling volume for super resolution is 0.5º by 0.25 km, an increase by a factor of 8 in resolution.

As a reference, bottom panels e and f of Fig. 3 show how the Doppler velocity measurements respond to constant reflectivity values (20 dBZ) across the EXP II vortex. With increasing range from the radar, the Doppler velocity profiles degrade in a consistent manner, with the peak value decreasing in magnitude and occurring at a greater distance from the vortex center. As expected, the degradation is more pronounced with legacy resolution than with super resolution.

With nonuniform reflectivity across the tornado, however, the Doppler velocity profiles behave differently as a function of range (middle panels c and d of Fig. 3). Within 20–30 km of the radar, the peak Doppler velocity values occur at a smaller radius than the actual core radius (thick gray curves). It is not initially evident why this should be the case, but apparently it is due to the presence of the weak–reflectivity eye.

The plots in Figs. 4–6 were prepared in order to help understand the anomalous behavior of the Doppler velocity profiles in Figs. 3c and d at a range of 10 km from the radar. The center of a horizontal cross-section through the radar beam is indicated by the black dot at the center of each panel. As one progresses through the top and bottom halves of the three figures, the radar scans across the EXP II tornado—starting with the beam centered on the tornado and ending with the beam centered 0.4 km from the tornado center. The four panels in each half of the three figures show, respectively, (a, e) the distribution of reflectivity within the range and azimuthal extent of the full beam, (b, f) the distribution of the radial component of raindrop velocities, (c, g) the distribution of reflectivity weighted by the two-way antenna beam pattern, and (d, h) the distribution of reflectivity–weighted radial velocity weighted by the antenna beam pattern. The mean Doppler velocity value within the beam is computed by dividing the sum of the values in panel d (h) by the sum of the values in panel c (g).

When the beam is centered on the weak-reflectivity eye of the vortex (Figs. 4a–d), significant concentrations of hydrometeors are found only at the far edge of both sides of the beam (Fig. 4a). Consequently, the radial velocity values that are sensed by the radar (Fig. 4d) occur beyond the core region (dotted circle in Fig. 4b) of the tornado. Because the positive and negative radial velocity values on both sides of the beam balance each other (Fig. 4d), the mean Doppler velocity within the beam is zero.

When the beam is centered 0.05 km to the right of vortex center (Figs. 4e–h), the concentration of scatterers is so small in the left portion of the beam (Fig. 4e) that the dominant reflectivity–weighted radial velocity values occur only in the right–most portion of the beam (Figs. 4g, h). The mean Doppler velocity value is assigned to the center of the beam, even though the mean value represents what is occurring along only one fringe of the beam. This, then, is the reason why the peaks of the mean Doppler velocity curves within a few tens of kilometers of the radar in Figs. 3c, d occur much closer to the center of the vortex than the true peak tangential velocities for an EXP II–size vortex.

The panels in Figs. 4–6 show that, as the beam center moves progressively away from the weak-reflectivity eye of the EXP II vortex, the locations of the radial velocity values that are represented by the mean Doppler velocity move progressively toward the center of the beam. When the beam center is 0.4 km from the center of the vortex (Figs. 6e–h), the main portion of the beam is outside the eye, so the mean Doppler velocity and reflectivity values are much closer to what they

would have been had the weak–reflectivity eye not been present.

4. DISCUSSION

With the prevalent use of mobile Doppler radars to make proximity measurements in tornadoes, it is important for users of the data to realize that they should use caution when interpreting Doppler velocity measurements. We have shown—through simulated Doppler radar measurements in a numerically–modeled tornado—that the apparent radius of maximum tangential velocities is underestimated when a prominent low–reflectivity eye is present in the radar measurements. As the low–reflectivity eye becomes less prominent (owing to decreasing tornado diameter or to a weakening tornado or to increasing distance between the tornado and radar), the apparent radius of maximum winds increases.

5. ACKNOWLEDGMENTS

Development of the numerical vortex model used in this study was supported by the National Science Foundation under Grant No. 0437898. Funding also was provided by NOAA/Office of Oceanic and Atmospheric Research under NOAA-University of Oklahoma Cooperative Agreement #NA17RJ1227, U.S. Department of Commerce.

6. REFERENCES

Alexander, C. R., and J. Wurman, 2005: The 30 May 1998 Spencer, South Dakota, storm. Part I: The structural evolution and environment of the tornadoes. *Mon. Wea. Rev*., **133**, 72–96.

Bluestein, H. B., and A. L. Pazmany, 2000: Observations of tornadoes and other convective phenomena with a mobile, 3–mm wavelength, Doppler radar: The Spring 1999 field experiment. *Bull. Amer. Meteor. Soc*., **81**, 2939–2951.

_____, W.-C. Lee, M. Bell, C. C. Weiss, and A. L. Pazmany, 2003: Mobile Doppler radar observations of a tornado in a supercell near Bassett, Nebraska, on 5 June 1999. Part II: Tornado–vortex structure. *Mon. Wea. Rev*., **131**, 2968–2984.

_____, C. C. Weiss, and A. L. Pazmany, 2004: The vertical structure of a tornado near Happy, Texas, on 5 May 2002: High–resolution, mobile, W–band, Doppler radar observations. *Mon. Wea. Rev*., **132**, 2325–2337.

Brown, R. A., B. A. Flickinger, E. Forren, D. M. Schultz, D. Sirmans, P. L. Spencer, V. T. Wood, and C. L. Ziegler, 2005: Improved detection of severe storms using experimental fine-resolution WSR–88D measurements. *Wea. Forecasting*, **20**, 3–14.

_____, V. T. Wood, and D. C. Dowell, 2006: Interpretation of simulated WSR–88D Doppler velocity signatures of tornadoes associated with nonuniform reflectivities. Preprints, *23rd Conf. on Severe Local Storms*, Amer. Meteor. Soc., St. Louis, MO, CD–ROM, P9.10.

Doviak, R. J., and D. S. Zrnić, 1993: *Doppler Radar and Weather Observations*. 2nd ed., Academic Press, 562 pp.

Dowell, D. C., C. R. Alexander, J. M. Wurman, and L. J. Wicker, 2005: Centrifuging of hydrometeors and debris in tornadoes: Radar–reflectivity patterns and wind–measurement errors. *Mon. Wea. Rev*., **133**, 1501–1524.

Fielder, B. H., 1993: Numerical simulation of axi-symmetric tornadogenesis in forced convection. *The Tornado: Its Structure, Dynamics, Prediction, and Hazards.* Geophys. Monogr. No. 79, Church, Burgess, Doswell, and Davies-Jones, Eds., Amer. Geophys. Union, 41-48.

Fujita, T. T., and R. M. Wakimoto, 1982: Anticyclonic tornadoes in 1980 and 1981. Preprints, *12th Conf. on Severe Local Storms*, Amer. Meteor. Soc., San Antonio, TX, 401–404.

Wakimoto, R. M., and B. E. Martner, 1992: Observations of a Colorado tornado. Part II: Combined photogrammetric and Doppler radar analysis. *Mon. Wea. Rev*., **120**, 522–543.

_____, W.-C. Lee, H. B. Bluestein, C.-H. Liu, and P. H. Hildebrand, 1996: ELDORA observations during VORTEX 95. *Bull. Amer. Meteor. Soc*., **77**, 1465–1481.

_____, H. V. Murphey, D. C. Dowell, and H. B. Bluestein, 2003: The Kellerville tornado during VORTEX: Damage survey and Doppler radar analysis. *Mon. Wea. Rev*., **131**, 2197–2221.

Wood, V. T., R. A. Brown, and D. C. Dowell, 2009: Simulated WSR-88D velocity and reflectivity signatures of numerically-modeled tornadoes. *J. Atmos. Oceanic Technol.*, in review.

Wurman, J., and S. Gill, 2000: Finescale radar observations of the Dimmitt, Texas (2 June 1995), tornado. *Mon. Wea. Rev*., **128**, 2135–2164.

_____, J. M. Straka, and E. N. Rasmussen, 1996: Fine–scale Doppler radar observations of tornadoes. *Science*, **272**, 1774–1777.

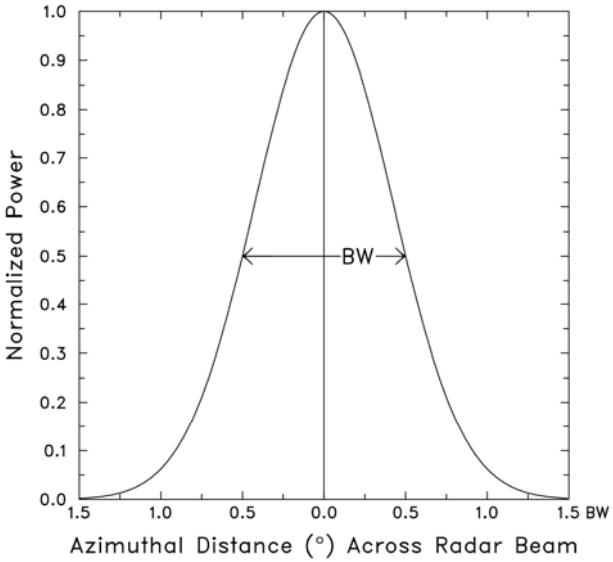

Fig. 1. Normalized power across the symmetric main lobe of a WSR–88D is approximated by the Gaussian distribution. The half-power beamwidth is indicated by BW. The portion of the main lobe of the beam used in our computations was three times the half-power beamwidth.

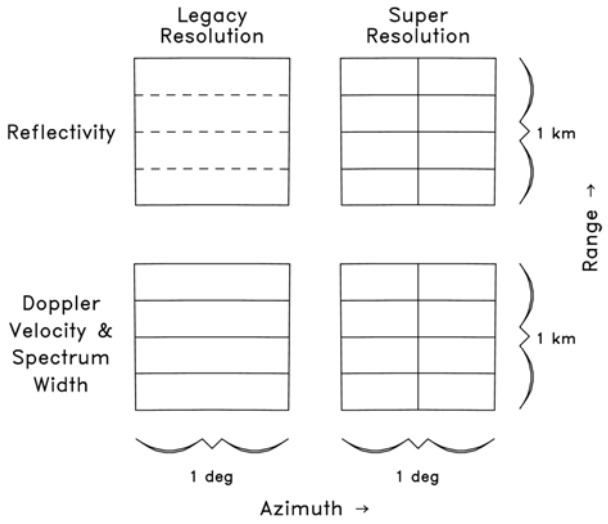

Fig. 2. Size of range gate bins (azimuthal width across page, pulse length up page) for legacy WSR–88D resolution (left column) and super resolution (right column) at a range of 60 km from the radar. Dashed lines in legacy reflectivity "rectangle" (1° by 1 km) indicate that four adjacent range gate bins of non-missing reflectivity values are averaged to produce the recorded and displayed reflectivity value. (After Brown et al. 2005)

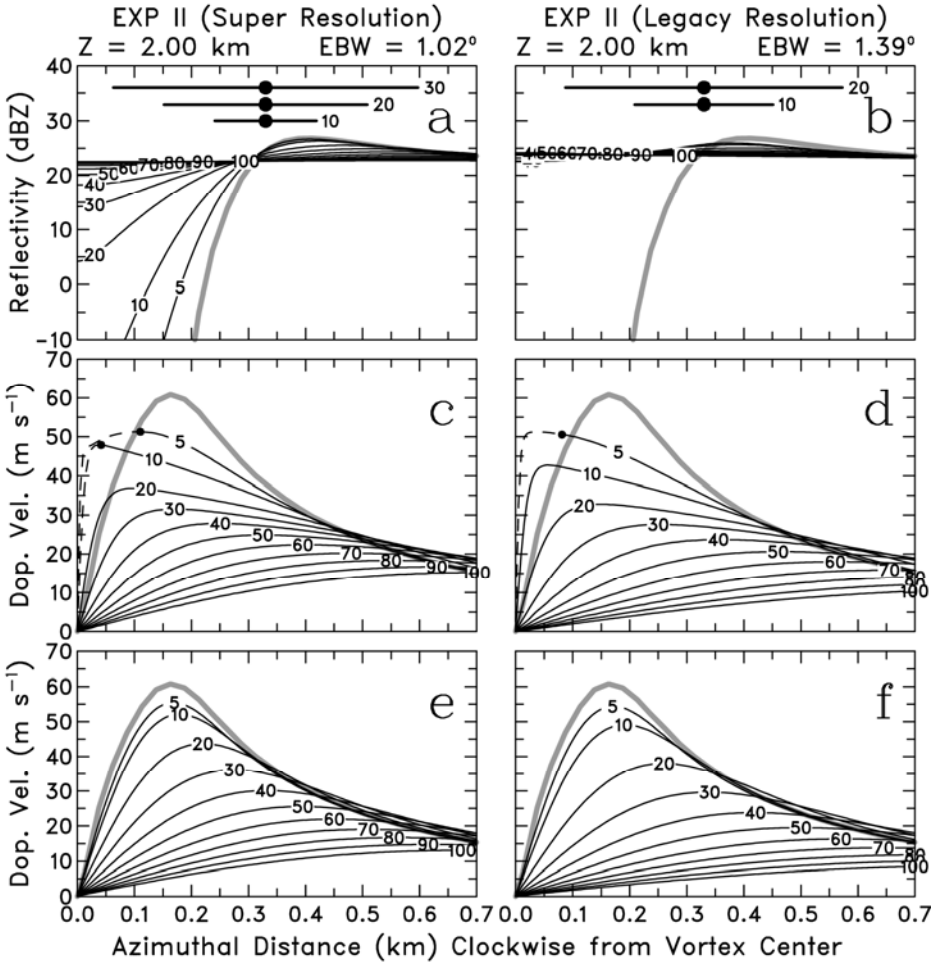

Fig. 3. Radial profiles of mean Doppler velocity and reflectivity from the tornado center for the large tornado (EXP II) at a height of 2.0 km and a variety of ranges from the simulated radar. The thick gray curves represent radial profiles of reflectivity computed directly from the model raindrop concentration (top panels) and of the tangential velocity of the model raindrops (middle and bottom panels). The horizontal lines with a center black dot in the upper portions of panels (a) and (b) represent the effective half-power beamwidth associated with ΔAZ = 0.5° (left column) and ΔAZ = 1.0° (right column) at the specified ranges (km). The black curves in panels (a) and (b) represent azimuthal profiles of radar reflectivity measurements at a number of different ranges (km) based on model reflectivity values as if the radar sampled the tornado in a continuous manner in an azimuthal direction. In the middle panels (c, d), the black curves represent Doppler velocity measurements computed from the model tangential velocity values and simulated nonuniform reflectivity values. The bottom panels (e, f) consist of Doppler velocity measurements calculated directly from the model tangential velocity values and a uniform reflectivity value of 20 dBZ that represents the initial concentration of raindrops in the numerical model. The small black dot between the solid and dashed portions of the curves in the middle panels represents the minimum detectable reflectivity value below which Doppler velocity values cannot be computed. The dashed portions of those curves represent the theoretical azimuthal profiles of Doppler velocity that would have been measured if there was no minimum detectable reflectivity value.

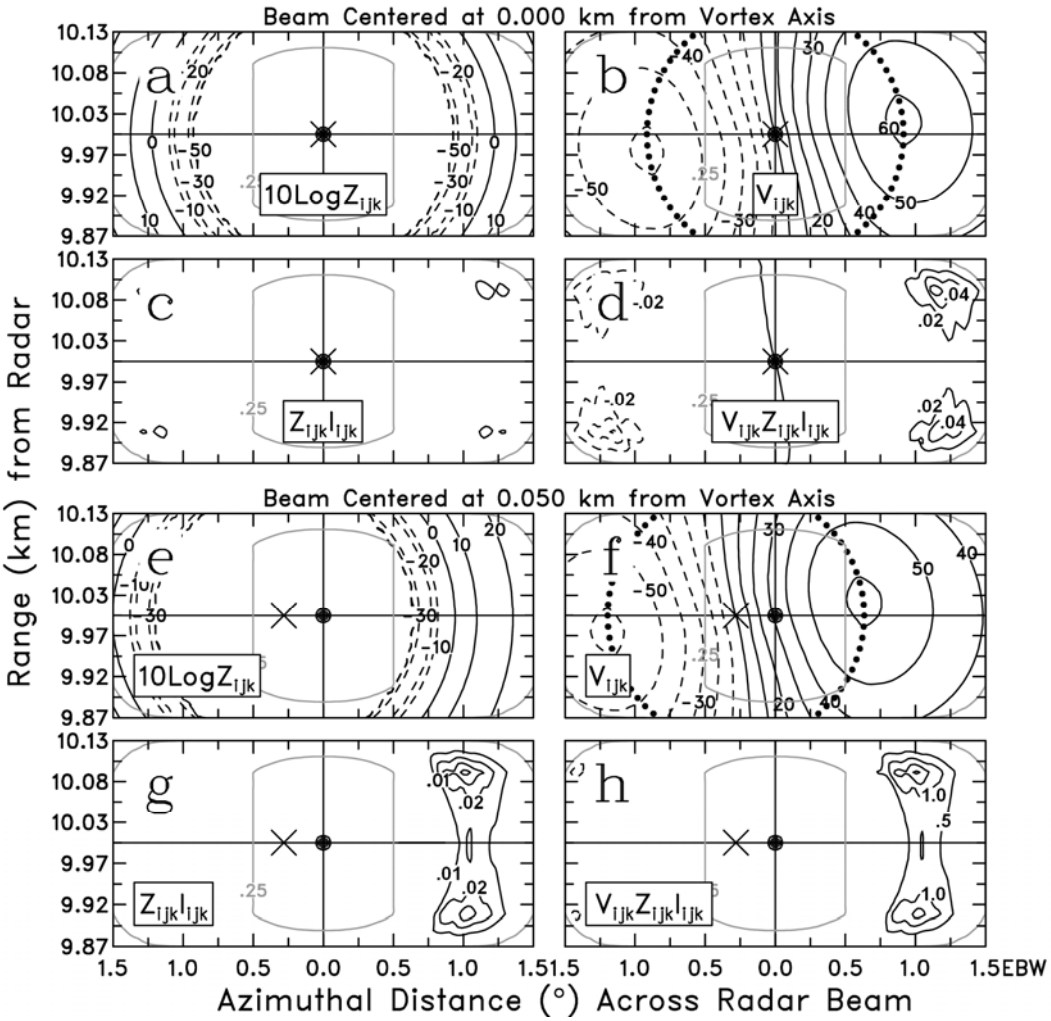

Fig. 4. Horizontal cross-section of the effective radar beam at 10-km range with the center of the beam (black dot) (a-d) coincident with the center of the EXP II vortex (X) and (e-h) located 0.05 km in a clockwise direction from the vortex center. Fields shown in (a, e) are distributions of model output of reflectivity (10 log Z_{ijk}, dBZ), (b, f) distribution of the radial velocity component of model raindrop motion (V_{ijk}, m s^{-1}), (c, g) product of reflectivity (Z_{ijk}) and composite antenna weighting function (I_{ijk}) of the antenna beam pattern (mm^6 m^{-3}), and (d, h) product of V_{ijk}, Z_{ijk}, and I_{ijk} (mm^6 m^{-2} s^{-1}). The mean Doppler velocity value within the beam is computed by dividing the sum of the values in panel d (h) by the sum of the values in panel c (g). Dashed and solid curves indicate negative and positive contours. The composite antenna weighting function is normalized to 1.0 at the center of the beam; gray contours represent normalized two-way antenna weighting values of 0.25 and approximately 0.0. Dotted black circle centered on X represents the location of true maximum hydrometeor tangential velocity in the panels (b) and (f). The positive (away from radar) and negative (toward radar) radial velocity peaks in (b) and (f) are not at the same range from the radar because hydrometeor motion in the vortex was slightly divergent.

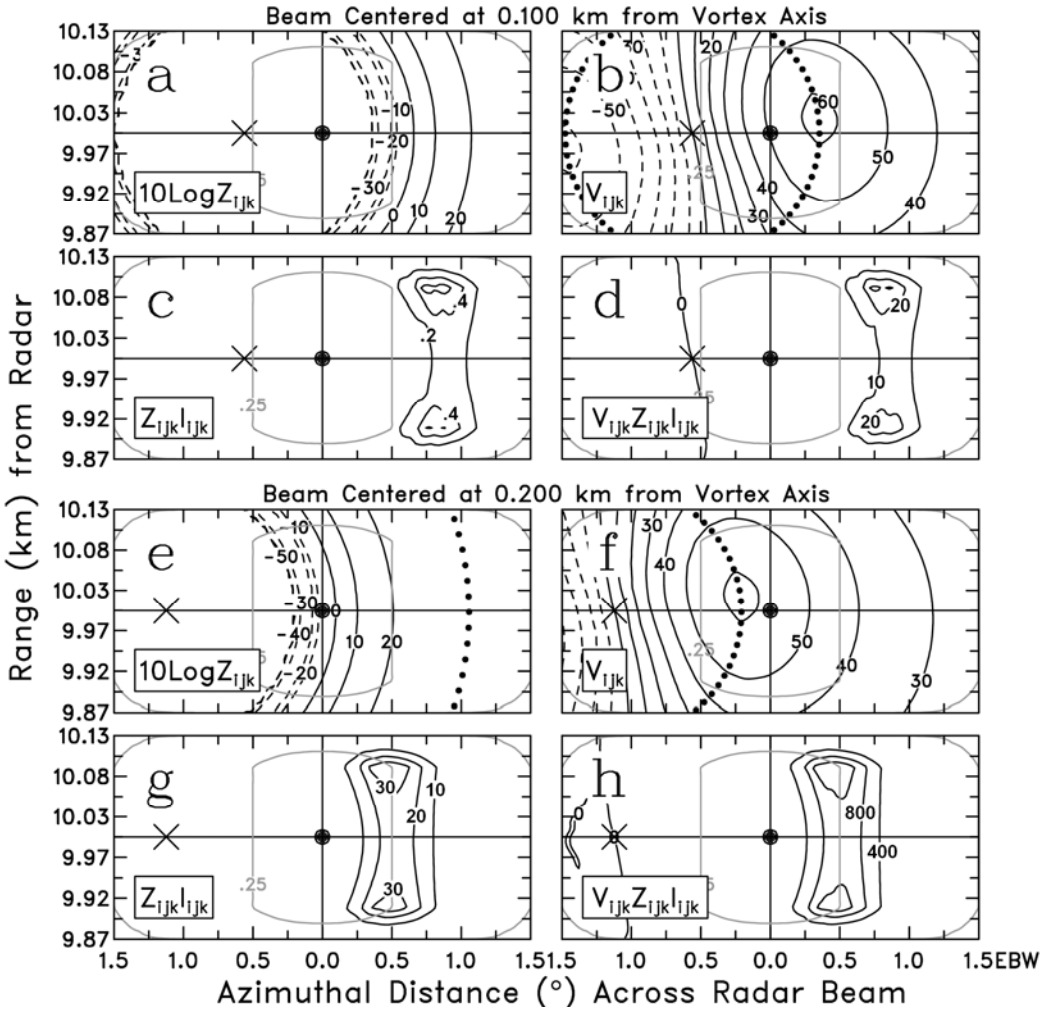

Fig. 5. Same as Fig. 4, except that the beam axis (black dot) is located (a-d) 0.1 km and (e-h) 0.2 km clockwise from the tornado center (X). The dotted black circle in panel (e) represents the location of the true maximum reflectivity in the annulus.

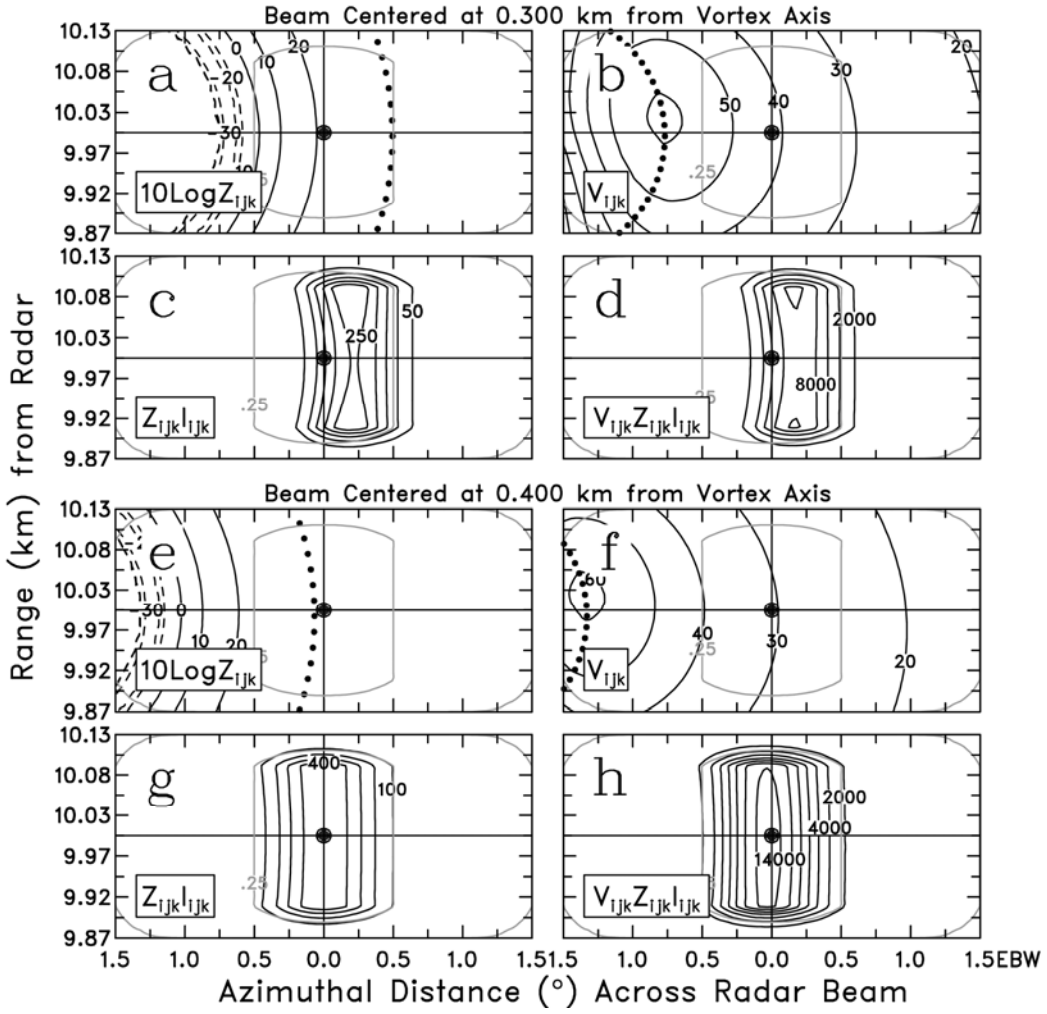

Fig. 6. Same as Fig. 4, except that the beam axis (black dot) is located (a-d) 0.3 km and (e-h) 0.4 km clockwise from the tornado center (X). The dotted black circle in panels (a) and (e) represents the location of the true maximum reflectivity in the annulus.